Proc. Indian Acad. Sci. (Engg. Sci.), Vol. 6, Pt. 4, December 1983, pp. 337–354.

Basic research problems in remote sensing

B L DEEKSHATULU and R KRISHNAN
National Remote Sensing Agency, Balanagar, Hyderabad 500037, India

Abstract. In this paper we describe the sources of geometric errors and methods to correct them with special reference to satellite-derived multi-spectral data. We then give an overview of an atmospheric model which can correct for atmospheric distortions. These are followed by discipline-oriented problems. We conclude by looking at some of the future remote sensing satellites which can cater to the problems referred to above.

Keywords. Atmospheric correction; remote sensing; geometric correction; multi-spectral data

1. Introduction

Remote sensing is primarily a tool; *albeit* a complex one. The present paper attempts to identify the deficiencies of this tool which limit its applications to different branches of science. Such a cataloging of the present limitations and shortcomings of remote sensing is necessary, not for discouraging its use but to refine this tool so that these deficiencies can be removed. It is not proposed to identify all basic research problems in this paper. Firstly two important problems are identified in some detail. All of remote sensing is faced with two problems: (i) the effect of the earth's atmosphere in obscuring and distorting the objects and (ii) the geometric and radiometric errors which corrupt the remotely-sensed data. In this paper we first describe the sources of geometric errors and methods to correct them with special reference to satellite derived multispectral data. We then give an overview of an atmospheric model which can correct for atmospheric distortions. These are followed by a brief mention of a few discipline-oriented research problems. We conclude this paper by taking a look at some of the future remote sensing satellites which can cater to the problems mentioned above.

2. Geometric correction of satellite data

The data received from a remote sensing satellite is geometrically inaccurate because of errors in the scanner, platform, ephemeris and attitude of the satellite in addition to errors due to earth's rotation, curvature and atmospheric refraction. While it is tempting to model all these errors and (along with accurate calibration measurements) correct for all these errors such an approach is infeasible mainly because of the difficulty of accurately measuring some of these errors like attitude errors. An alternate approach is to register this data with a corrected image using ground control points. Such an approach is feasible but costly because of the large number of ground control points (GCPs) which would be required. Automatic identification of GCPs and correction still remains a formidable task.

A judicious combination of the above two approaches seems the best solution. After correcting the data using models for the different sources of errors, further refinement can be carried out using GCPs.

In the following we illustrate the different errors and the modes of corrections.

2.1 *Earth rotation, curvature and panoramic distortion:*

The rotation of the earth, its curvature and panoramic effects cause distortions in the imagery. The earth rotation effect is compensated by shifting scan lines in a west-east direction. Figure 1 shows the earth curvature and panoramic distortion effects. The correction for the ith pixel is

$$C_i = \frac{\theta_i}{\Delta\theta_i} - \frac{\phi_i}{\Delta\phi}$$

where $\Delta\theta = \theta_{max}/N$ and $\Delta\phi = \phi_{max}/N$ and there are $(2N+1)$ pixels per scan line. θ is the scan angle and ϕ is the central angle.

2.2 *Line length correction*

The time taken for a mirror scan can vary due to imperfections in the electromechanical drive system. But the electronic sampling of the data is done at an uniform rate. This results in the number of pixels being different from the nominal. If scan lines have different number of pixels the picture will have a jagged appearance. To correct this, all the scan lines are made to have the same number of pixels by counting the pixels in the line length and distributing the excess or deficit uniformly along the scan line.

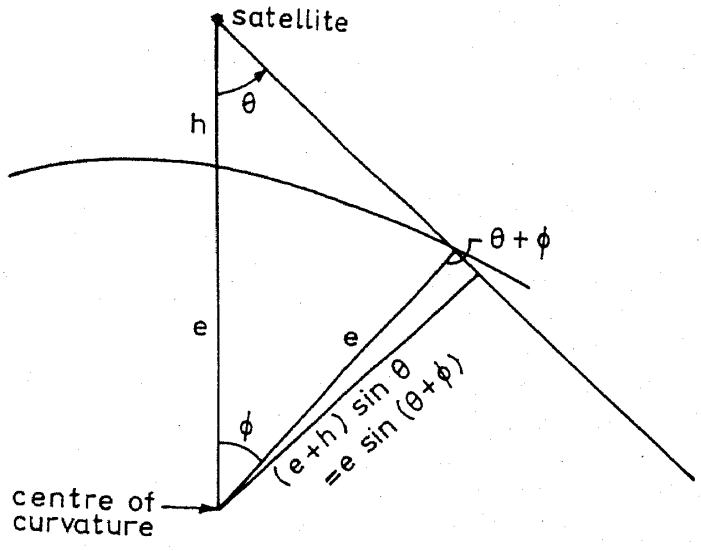

Figure 1. Scan geometry

2.3 *Mirror scan nonlinearity*

The multispectral scanner mirror's scanning rate is not constant. It varies nonlinearly due to the imperfect nature of the electromechanical driving mechanism. The mirror velocity is not constant because of the speeding up at the beginning and slowing down at the end of scans. It is more nearly represented by a cosine function. Because of the varying velocity, the pixel elements overlap to varying degrees on the ground. To correct for this, the input location is computed using the cosine curve for each output pixel location and its radiometric value is calculated using the nearest neighbour or cubic convolution methods.

2.4 *Ephemeris errors*

Errors due to wrong prediction of the satellite position can be corrected only with ground control points. This will be discussed later.

2.5 *Attitude errors*

By the attitude of a spacecraft at a given time is meant the orientation of the spacecraft coordinate axes, called the body axes. The axis along the velocity vector is called the roll axis, the axis perpendicular to the velocity is called the pitch axis and the third axis which completes the coordinate frame is called the yaw axis (figure 2). The rotation of the spacecraft about these axes gives rise to the altitude errors and if these are not taken care of then the ground scene 'seen' by the satellite will be different from what is predicted based on the satellite's position alone. The errors which can result from these three altitude distortions are shown in figure 3.

The attitude of the satellite is sensed by gyros and other sensors and transmitted to the ground in the earth-centred inertial coordinate system (figure 4) in the form of Euler quaternious. The X axis in figure 4 points towards the first point of Aries, the Z axis is towards the North and the Yaxis completes the coordinate system. Figure 5 shows the correction geometry. The vector OT is obtained by solving the triangle OTS. E is computed from the Euler quaternions and R from the ephemeris data.

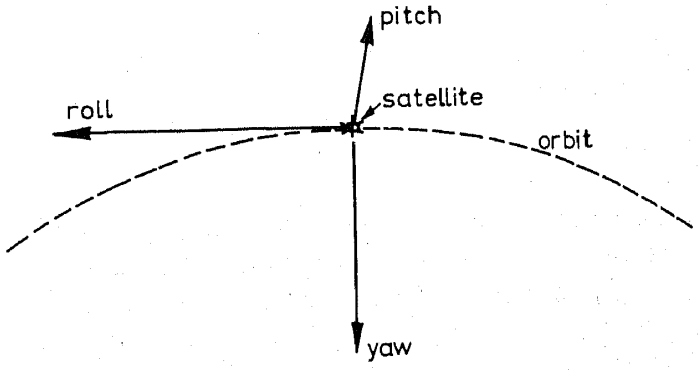

Figure 2. The pitch, roll and yaw axes

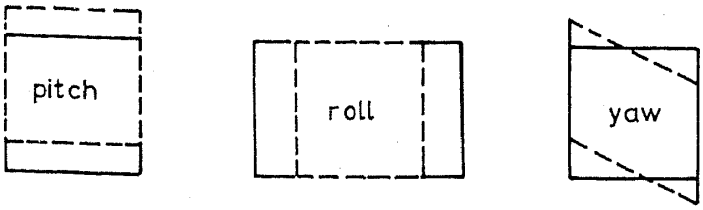

Figure 3. Distortions due to attitudinal changes

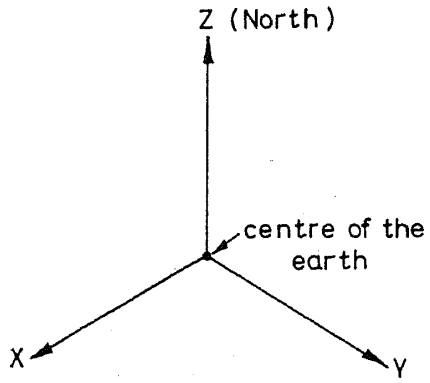

Figure 4. The earth-centred inertial true of date system

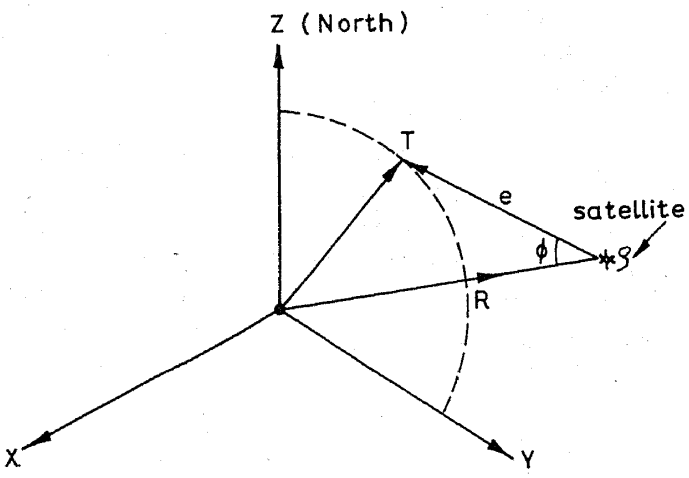

Figure 5. Altitude correction

3. Use of GCPs in correction

The preceding paragraphs describe some of the sources of geometric inaccuracy and indicate ways of correcting these errors. One would assume that one can measure all the geometrical parameters using accurate calibration techniques for the sensor, positioning system and attitude measurements, refraction model for the atmosphere and a digital terrain model for the relief. However it is impossible to achieve good accuracy with this approach, mainly due to the inaccuracy of attitude measurements.

A diametrically opposite approach is to register an image over a map or another image without any information on its *a priori* geometry. Many pairs of image points corresponding to the same ground point have to be located in both images. The geometric correction problem can then be viewed as a registration problem.

3.1 *Location of* GCPs:

A GCP is a point which is visible both in the image and a reference map or aerial photograph. An image control point can be identified on several images of the same area. One of the images is the reference for which the coordinates are known. For the other images it is possible to find their coordinates using correction techniques (Baudoin *et al* 1981)

3.1a *Preprocessing for correlation* The image is transformed into a binary matrix (0, 1) by spatial filtering and thresholding. For example the pixel P_{ij} is transformed into b_{ij} as

$$b_{ij} = 0 \quad \text{if} \quad (P_{ij} - P_{(i-1)j})^2 + (P_{ij} - P_{i(j-1)})^2 < S,$$

where S is a threshold. For finding the actual location of the ground control point a search binary window from the corrected image is taken and placed at different positions on the image to be corrected. A correlation parameter is computed by counting the number of common 1's. The GCP is located at the point of maximum correlation (Baudoin *et al* 1981)

3.2 GCP *file*

It is necessary to evaluate the relative usefulness of different types of GCPs like road intersections, river intersections, coastline points etc. The fully automatic identification and correlation of GCPs with image points is still a formidable task. At present only an interactive identification followed by automatic correction seems feasible.

3.3 *Geocoded data*

While correcting satellite data as such or registering it to other corrected images is desirable, because of the different types of satellite data available to the user it would be desirable to register the different types of data to a common topographic grid. Such a data is referred to as geocoded data. The Canadian Centre for Remote Sensing has generated such data.

4. Geometrical errors affecting classification

Errors due to misregistration, noise, spatial transient response, field size etc cause classification errors. For example if the pixel size is not small enough a single pixel may contain more than one object and will either be misclassified or may fall outside the classification limit. Nalepka *et al* (1972) have shown that if two classes which are

supposed to be averaged by a pixel have the same covariance matrix then the proportion of the classes can be estimated by solving a quadratic assignment problem. Krishnan & Natarajan (1978) have given a heuristic solution to this problem which assumes that the proportions are proportional to the conditional densities of the two classes. While the misregistration effects are prominent at the boundaries between classes, even field-interior pixels are non-uniform because of the combined effects of sensor noise and inherent non uniformities in the field itself. The probability of a sample being within its class limits can be derived by assuming that any ensemble of noise-free signals from a series of areas of the same material can be anywhere within the quantizing range with uniform probability, but that individual samples are perturbed by the Gaussian noise with a distribution equal to σ. The probability distribution of the signal plus noise is found by convolving the probability distribution of the signal with that of the noise. The probability of correct class assignment is then found by integrating the probability distribution between appropriate class limits (Friedman 1966). The result of this classification is shown in figure 6.

Billingsley (1982) shows that the curve can be approximated by $\beta \log P = -0{\cdot}4$ for the range $3 \leqslant \beta \leqslant 7$. As an example consider a scene having a field-interior variation of 3% and sensor noise of 1% (Billingsley 1982). The total effective noise seen by the classifier will be the RMS sum of these two which equals 3·16%. In terms of digital values this becomes $3{\cdot}16 \times 256/100 = 8{\cdot}1$. If the class width is 25 then $\beta = 3{\cdot}1$ and $P = 0{\cdot}742$. If the 2×2 pixels are averaged then $\beta = 6{\cdot}2$ and $P = 0{\cdot}86$. Therefore, while small pixels are needed for class separability, large pixels (or averaged pixels) are less susceptible to noise. This is the basis of the per field classification proposed by Fu (1983). Here a group of pixels is classified by using their distribution and the distance between density functions. However Billingsley's analysis shows that it is preferable to go in for small pixels if smaller fields are of importance.

5. Effect of local solar time on classification accuracy

Since the LANDSAT satellites are sun synchronous, data is always collected at approximately the same local solar time. Because of this the effects of different local solar times on class separability has not received much attention. However with the increase in the number of remote sensing satellites it may be necessary to schedule these at different local solar times (LST) to avoid data reception conflicts. Table 1 which gives the distinguishability at different LSTs, is based on a study carried out in the United States (Malila *et al* 1974).

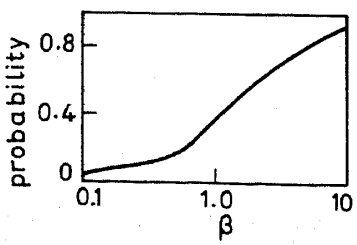

Figure 6. β vs probability

Table 1. Effect of local solar time on classification accuracy

Classification Run	LST	% Correct classification Corn	Trees	Hay	Oat	Beans	Soya beans	Avg.
1.	9:33	83·3	87·6	77·4	81·1	95·2	99·1	84·4
2.	10:07	80·1	89·3	90·2	55·8	95·2	97·5	82·8
3.	10:55	80·6	90·8	87·6	85·2	95·0	98·4	87·6
4.	11:33	75·4	87·2	84·8	82·8	96·0	87·6	83·5
5.	13:56	85·4	90·0	85·7	90·5	90·8	98·6	87·7
6.	14:50	79·1	91·5	86·4	87·2	96·3	90·0	86·1

It can be seen that if the anomalously low accuracy for data at 10:07 LST is ignored, the classification accuracy of all the crop types increases till about 11:00 and then decreases as solar noon is approached.

6. Effect of the atmosphere on remote sensing

The atmosphere attenuates and distorts the signal coming from the earth's surface to the remote sensing sensor. The gases and aerosols present in the atmosphere scatter, absorb and emit radiant energy. The atmosphere is transparent in certain narrow regions of the visible, infrared and microwave regions. The atmosphere is practically opaque in the ultraviolet (shorter than 0·32 μm) and hence the ultraviolet is not suitable for remote sensing. Table 2 (Fraser *et al* 1976) shows the atmospheric windows available for remote sensing.

The atmospheric windows important for remote sensing range from 1·5–1·8, 2·05–2·4, 3·5–4·1, 4·5–5, 8–9·2 and 10·2–12·4 μm. The region between 1·5 and 1·8 μm is useful for leaf moisture change detection. For forest fire detection the band 3·5 to 5 μm is useful. The main source of electromagnetic energy reaching the earth is the sun. The maximum irradiance of the sun occurs at 0·47 μm. For wavelengths longer than 4 μm, the earth and the atmosphere are the main sources.

The atmosphere either scatters, absorbs or emits radiant energy. The Rayleigh or molecular scattering is dominant in the visible and near-ultraviolet regions and increases with the inverse fourth power of the wavelength. Thus it is very severe in the ultraviolet and causes the blue colour of the sky. N_2 and D_2 are the main molecular scatterers. CO_2 has many absorption bands and can influence atmospheric absorption even when in trace quantities. Water vapour also has a prominent role in absorption.

The negative logarithm of the transmittance is called the optical thickness τ. Consider a beam of light of wavelength λ travelling through the atmosphere in a

Table 2. Major atmospheric windows available for spacecraft remote sensing (value in μm)

Ultraviolet and visible	0·3–0·75; 0·77–0·91
Near-infrared	1–1·12, 1·19–1·34; 1·55–1·75, 2·05–2·4
Mid-infrared	3·5–4·16, 4·5–5·0; 4·5–5
Thermal infrared	8·0–9·2; 10·2–12·4; 17·0–22
Microwave	2·06–2·22; 3–3·75; 7·5–11·5; 20

direction θ with respect to the earth's surface normal. After travelling a distance l, the spectral radiant flux ϕ (1) can be related to its initial value

$$\phi_\lambda(0) \text{ by } \left(\exp \frac{-1}{\cos\theta} \int_0^1 K_\lambda(Z)\,dz\right)\phi_\lambda(0),$$

where $z = 1\cos\theta$ and $K_\lambda(Z)$ is the attenuation coefficient. The quantity

$$\int_0^z K_\lambda(Z)\,dz = \tau_\lambda(Z)$$

is called the optical thickness and

$$\exp\left(-\int_0^z K_\lambda(Z)\,dz\right) = T_\lambda(Z)$$

is called the beam transmittance (Sturm *et al* 1981).

$$K_\lambda(Z) = K_\lambda^M(Z) + K_\lambda^A(Z),$$

where M and A stand for molecules and aerosols respectively.

$$K_\lambda(Z) = N^M(Z)\,\sigma_\lambda^M + N^A(Z)\,\sigma_\lambda^A,$$

where $N(Z)$ = number of particles/unit volume at height Z, σ_λ = cross-section, $\sigma_\lambda^M = \sigma_{\lambda s}^M + \sigma_{\lambda a}^M$, and $\sigma_\lambda^A = \sigma_{\lambda s}^A + \sigma_{\lambda a}^A$, where s and a stand for scattering and absorption. From Rayleigh's theory

$$\sigma_{\lambda s}^M = 8\pi^3(n^2-1)^2/3N^2\lambda^4,$$

where n is the refractive index for air at standard conditions, N is the molecular number density at standard conditions.

The scattering by aerosol particles can be explained by Mie scattering (Sturm *et al* 1981). The cross-sections depend on the geometric cross-section πr^2 of the particle and certain efficiency factors.

Absorptance calculation Having given a general overview of the atmospheric scattering and absorption phenomena, we now describe briefly the different classes of methods used to calculate absorptance. These can be classified as (i) line-by-line method (ii) aggregate method (iii) LOWTRAN-2 and (iv) multiparameter analytical. The following treatment is from La Rocca (1975).

6.1 *Line-by-line method*

The atmospheric transmittance at different frequencies is shown in figure 7 (La Rocca 1975). If one of the lines is observed free from the influence of the other lines the shape

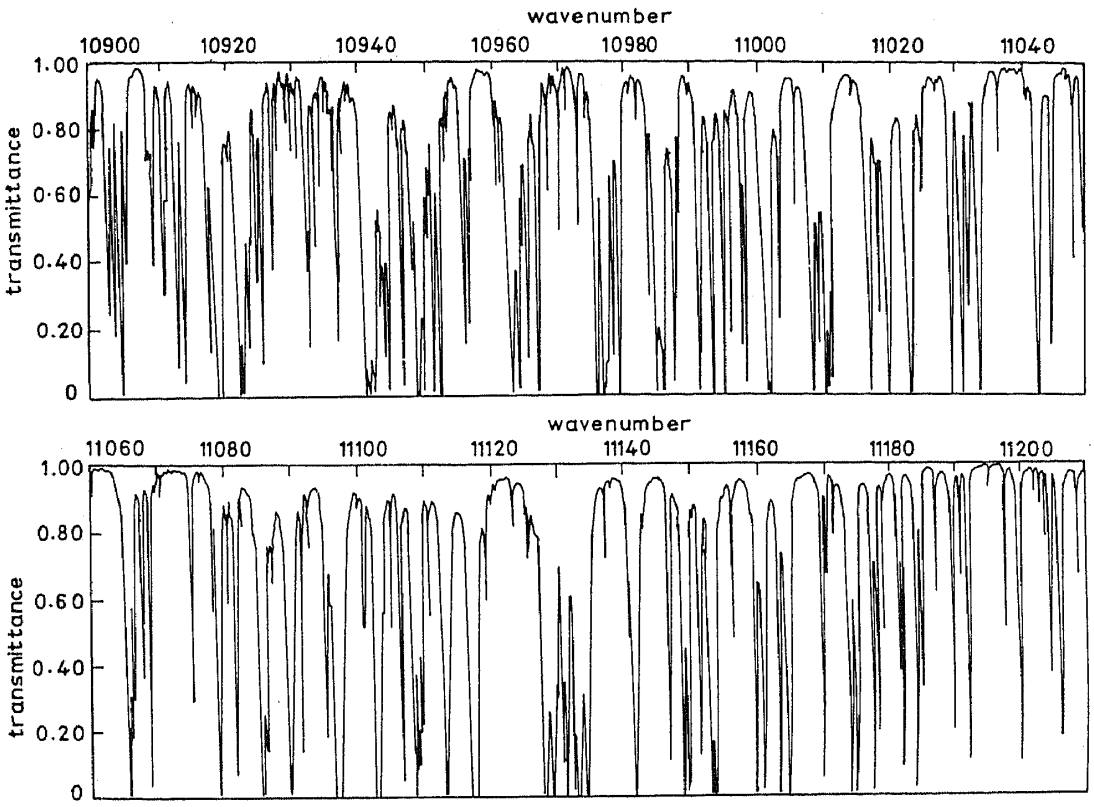

Figure 7. Atmospheric transmittance due to molecular absorption through a 10 km horizontal path at sea level.

will be as shown in figure 8 (La Rocca 1975) where $K_a(\gamma)$

$$\frac{S}{\pi}\frac{\alpha_L}{(\gamma-\gamma_0)^2+\alpha_L^2}=K(\gamma)$$

where S = line strength in g^{-1} cm· α_L = the Lorentz half-width in cm^{-1}, defined as half

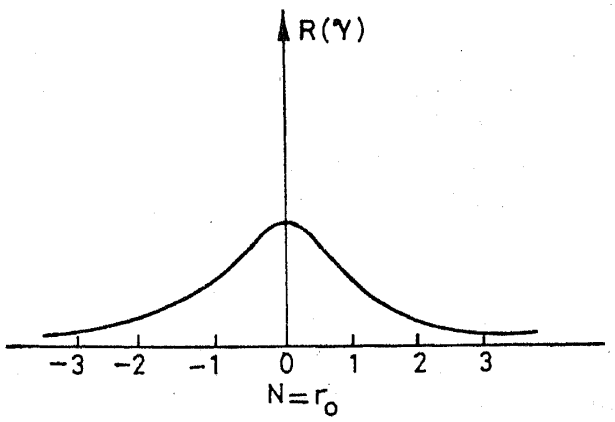

Figure 8. Lorentz shape

the width of the line at half the max value of $K(\gamma)$ and $(\gamma - \gamma_0)$ = the separation in cm^{-1} between the arbitrary frequency γ and the line centre γ_0.

The Airforce Cambridge Research Laboratories (AFCRL) have compiled a set of parameters that describe the molecular lines in which radiation is absorbed and emitted. This table forms the basis of the line-by-line method. The basic idea behind this method is to calculate the transmittance at a pre-determined frequency and numerically integrate over the $\Delta\gamma$ corresponding to the spectral resolution for which the transmittance is desired. The transmittance for a path s from the contributions of n lines at γ is determined from

$$\exp\left[-\int_0^s \sum K_i(\gamma, P, T)\,\rho_i\,\mathrm{d}s'\right],$$

where P and T refer to the pressure and temperature and ρ is the number of molecules per cm^3. The line-by-line method is highly time-consuming. Even with the time-saving approximations it is still prohibitively expensive.

6.2 *Aggregate model*

The aggregate model makes use of what are called 'band' models. In the formulation of a band model it is necessary to postulate a generalized structure for the lines in a particular infrared region. For example the Elsasser model assumes that the lines are regularly spaced. Then we have

$$k(\gamma) = \sum_{i=-\infty}^{\infty} \frac{S}{\pi} \frac{\alpha_L}{(\gamma - i\delta)^2 + \alpha_L^2},$$

where, for δ equal to the mean spacing between line centers, $i\delta$ is the position of the ith line centre. Using this value and integrating over one cycle of the regular pattern we get the transmittance. The aggregate method is a compilation of the various band models.

6.3 LOWTRAN-2

The LOWTRAN is perhaps the most widely used model. This is an empirical method, deriving its functional form from experimental investigations and from tabulated data in the AFCRL compilation. A series of prediction charts giving the empirical transmittance function for H_2O, O_3, CO_2, N_2O, CO, CH_4, O_2 and their mixtures, forms the basis of this method. Once the equivalent absorber amount is known the transmittance for any environmental condition can be determined.

6.4 *Effect of atmosphere on classification*

Numerous experiments conducted at the Purdue University and at Environmental Research Institute of Michigan (ERIM) indicate that, if the optical characteristics of the atmospheres over an unknown scene and over the region of the truth set are uncorrelated and differ in aerosol mass by two standard deviations, misclassification errors of 20–30 % can appear when maximum-likelihood classification algorithms are

used (Fraser *et al* 1976). These methods are represented by actual analytical functions rather than empirical models.

6.5 *Effect of atmosphere on infrared radiation* (Baudoin *et al* 1981)

The effect of atmosphere on the infrared sensor performance is different in two significant ways from the effect of the atmosphere on a sensor operating in the visible part of the spectrum. Firstly the atmosphere is transparent only in limited intervals in the infrared. Secondly as a consequence of the peak at $\sim 10\ \mu m$ in the blackbody radiation curve for objects at terrestrial temperatures the atmosphere must be considered a source of radiation throughout most of the infrared spectral region.

The atmosphere should be divided at about 70 μm into two altitude regions because of the difference in the physical processes that are important to radiation above and below this altitude. In the lower atmosphere molecules collide frequently to establish a thermodynamic equlibrium. In the upper atmosphere there is no thermodynamic equilibrium and all the various excitations and relaxation processes involving chemical reactions, collisions and photons must be considered in detail.

The infrared atmospheric transmittance features are shown in figure 9. Considering molecular absorption, the gases that absorb in the near infrared are H_2O, CO_2, O_3, N_2O, CO, CH_4 and HNO_3 and in the far-infrared O_2. H_2O and O_3 are very unevenly

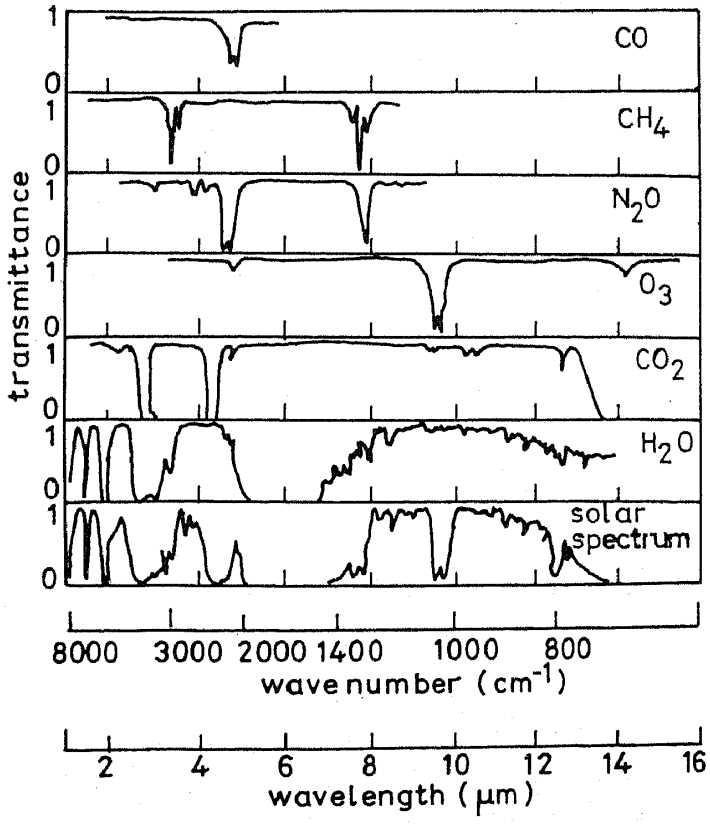

Figure 9. Near- and mid-infrared transmittance spectra of a number of gases occurring naturally in the atmosphere. A spectrum of the transmittance of solar radiation through the atmosphere is also shown to illustrate the importance of these minor constituents of the atmosphere in a discussion of infrared atmospheric effects.

distributed in the atmosphere. The effect of varying water vapour concentrations on transmittance is shown in figure 10.

Considering aerosols, as in visible radiation, the atmospheric aerosols are poorly defined in terms of particle size distribution, shape etc and this makes the application of Mie theory difficult.

Infrared cloud images can give a lot of information. The temperature of the cloud can be estimated from the infrared radiation and hence the altitude.

7. Application specific problems

It is necessary to develop models which will correct the anisotropic reflectances in remotely-sensed images from mountainous regions covered with vegetation. The anisotropic reflectances are further complicated by variable surface orientations (Hugli & Frei 1981). Earlier studies on the anisotropic reflectance problem assumed that the orientation does not affect the reflectance. Recent studies showed that the approach is feasible only for non-vegetated surfaces. It is necessary to refine the model.

7.1 *Detecting forest disturbances by incorporating* DTM *information*

Recently it has been proposed that by incorporating digital terrain model information, the confusion between spectrally similar forest canopy conditions such as healthy vegetation and moderate defoliation can be resolved. Studies to determine relationships among severity of defoliation, slope orientation, and spectral response have to be conducted for different kinds of defoliation (in the US gypsy moth defoliation has been

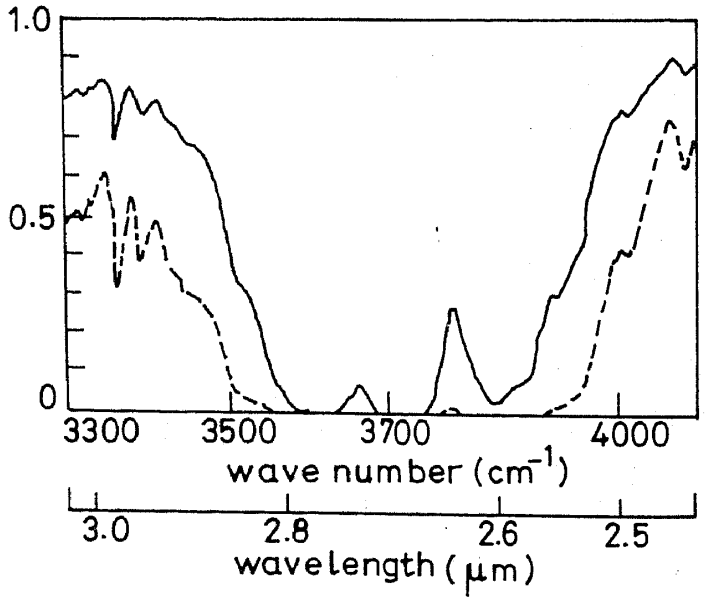

Figure 10. Low-resolution atmospheric transmittance spectro-computed for the same optical path but different atmospheric conditions. The dashed curve is a moist, tropical atmosphere and the solid line is for a very dry, subarctic winter atmosphere. Both calculations were made with the LOWTRANZ program for an optical path from 5 km to space at a 60 day zenith angle.

studied extensively). For example areas of moderate defoliation on southeast aspects are spectrally similar to healthy forests on northwest aspects.

7.2 *Geology and geophysics*

7.2a *Enhancement of lineaments* Active faults seen in LANDSAT images are mainly analysed visually even today. If this procedure can be automated, it would give us valuable results, *viz* exclusion of subjectivity by analysts, release from voluminous work etc. Since direct machine processing of faults is very difficult, lineaments are generally taken as the target in place of the fault. Some attempts have been made to identify and enhance lineaments. These involve semilinear line detectors, global edge detection, matched filtering etc. Attempts have to be made to further improve these methods. Also a recent study indicates that the texture of lines near a fault could give some indication of the existence of the faults. This needs further investigation. Fuzzy lineament extraction algorithms have not been tried at all.

7.2b *Structural Analysis of geological phenomena using simulated illumination conditions of satellite data* Recent studies have indicated that if the satellite data can be viewed under different lighting conditions geological features could be enhanced. For this a digital terrain model has to be incorporated with LANDSAT data and for each pixel, taking the sun elevation angle, new intensities have to be calculated. Shading also can be incorporated to enhance geologic structures.

7.2c *Problems in oil and gas exploration* (Short *et al* 1975) The following points restrict the use of surface remotely-sensed data in oil and gas exploration:

(i) Surface indications of oil and gas are relatively rare and most have probably been detected in the more accessible parts of the world.
(ii) Today, most new oil discoveries are being made primarily through the use of geophysical methods and by drilling in as much as the most decisive data now needed relates to deeply buried subsurface conditions that generally have poor surface expression.
(iii) The precise role of linears in localizing oil has not been fully established, depends on time of formation, depth to producing zone(s), caprocks characteristics etc.
(iv) Geological complexities (unconformities, glacial cover etc) unrelated to petroleum accumulation frequently mask oil and gas traps.
(v) The hypothesis that hydrocarbons can escape to the surface and cause recognizable alteration effects is unproved; the rate of escape may be less than the rate of surface erosion or other removal factors.
(vi) It is difficult to assess man's role or that of vegetation in producing (or observing) tonal and hazy anomalies.

7.2d *Gaseous pollution monitoring* (Otterman *et al* 1975) The weakness of pollution monitoring from LANDSAT imagery is that a specific identification of a pollutant is not on spectral signature. The identifications are based generally on the fact that the identified pollutant is the only likely incident for a particular location. A sensitive technique for detecting and measuring the concentration of a specific gaseous constituent is correlation spectroscopy. This method is particularly suitable for gases with absorption

bands with pronounced multiple peaks and troughs, such as the 0·3 μm absorption band of SO_2. A mask is applied to the measured spectral radiances in such a way that only two readings are taken; one is the sum of the radiances at wavelengths corresponding to absorption, and the other is the sum of the radiances at wavelengths corresponding to the troughs. The differences between these two readings divided by their sum depends on the product of the pollutant concentration and path length. Correlation spectrometers should be incorporated in remote sensing platforms. A further problem in the identification of N_2O, NO_2, SO_2, H_2S and HNO_3 is that masking absorbers like H_2O, CO_2, O_3 and CH_4 hinder their identification. Spectroscopic techniques usually need a long dwell time. This poses an additional problem in their incorporation into remote sensing platforms.

7.3 *A problem in weather monitoring* (Tepper *et al* 1975)

Present activity in the use of remote sensing has focussed on the medium scale weather phenomena (figure 11). On the short end of the scale are severe local storms characterized by a short time interval and limited aerial extent. Here it is felt that geostationary satellites like INSAT will be most useful and our future development should consist of major improvements in the existing geostationary satellites. The first of these will be the incorporation of a sounder on board a geostationary satellite. This will permit us to investigate the details of the environment in which severe local storms breed. At the other end of the scale is the climate variation scale. This includes snow, ice, sea conditions and solar constant and the measurement is a complex task.

7.4 *Estimating green biomass*

Estimating standing biomass is an important problem in rangeland management. The reflectance from the vegetation canopy is influenced by varying soil reflectance, biomass, percent vegetation cover, leaf area index, canopy structure, amount of live and dead vegetation, solar zenith angle, look angle and azimuth angle (Colwell 1974).

7.5 *Vegetation cover leaf area index and biomass* (Colwell 1974)

There are three leaf area indices (LAIS), called horizontal, vertical and total. Horizontal LAI is the amount of horizontal components of leaves projected onto the ground. The

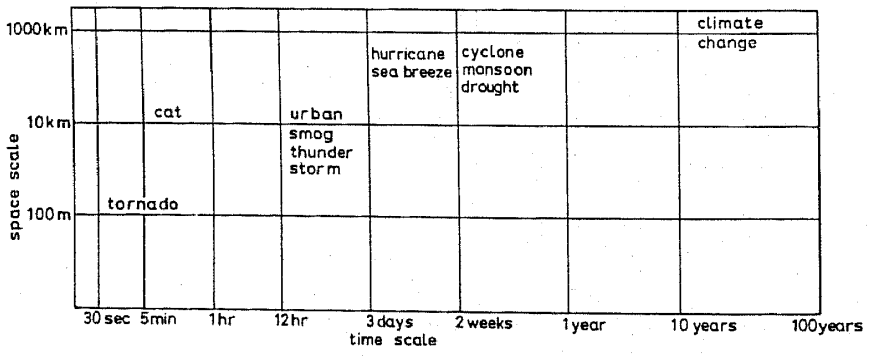

Figure 11. Meteorological phenomena.

vertical LAI is similarly the components perpendicular to the ground. The biomass is the total weight of standing vegetation over an unit area of ground. Vegetation cover is the proportion of ground area obscured by vegetation when looking straight down. The per cent of vegetation cover for an area with horizontal LAI = H can be approximated by $1-\exp(-H)$.

Table 3. Horizontal LAI and leaf cover

Horizontal LAI	$1-\exp(-H)$
1	0·63
2	0·86
3	0·95
4	0·98
5	0·99

Figure 12 indicates the change in reflectance for increasing the total leaf area index. The red reflectance is quite sensitive to LAI at small values of LAI. The red reflectance becomes virtually insensitive to further increases in LAI at much lower values of LAI than those at which the near infrared reflectance becomes insensitive.

7.6 *Vegetation index* (Colwell 1974)

The ratio (IR − red)/(IR + red) is referred to as the vegetation index (VI). VI has been found to exhibit a direct relationship with the green material present. Tucker *et al* (1979) report that both for corn and soybeans VI depicted the stages of growth accurately. Before crop emergence VI is negative. With increasing crop cover VI increases rapidly. Once the crop cover is complete VI reaches a plateau. Then VI declines gradually

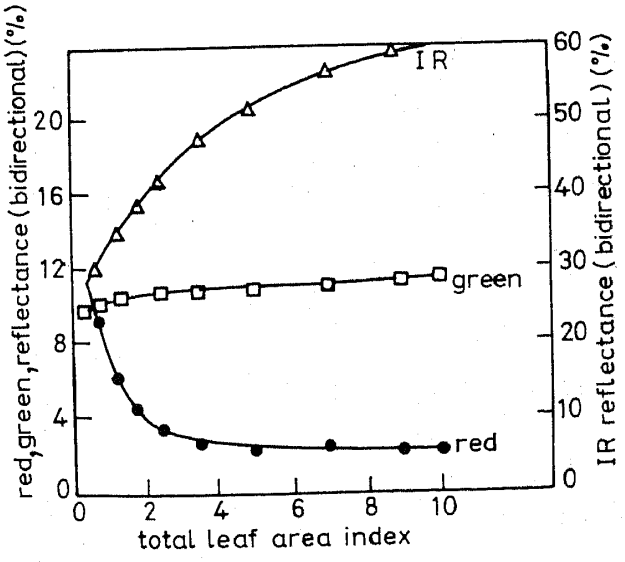

Figure 12. Bidirectional reflectance of simulated canopies with light soil. Look angle $\phi = 0°$ solar zenith angle $\theta = 20°$.

as harvest season approaches. Chlorophyll density and green-leaf biomass affect VI. Drought would affect the VI by limiting plant growth such that the plateau would be reached at a later date or a lower level would be attained. High fertility of soil would elevate and low fertility would depress VI.

7.7 *Effect of solar zenith angle* (Colwell 1974)

Table 4 shows the change in canopy reflectance for a change in solar zenith angle. The reflectance changes rapidly with the solar zenith angle. The reflectance changes are not even proportional in the different bands since the changes are largely a function of the relative darkness of the shadow. Shadow darkness is a function of leaf transmittance which is different for the different lands. Even ratioing of IR and red as is done with VI cannot eliminate the effect of solar zenith angle.

Table 4. Effect of zenith angle on change in canopy bidirectional reflectance for a 0° look angle ($V/H = 2/1$)

Zenith Angle	Green	Red	IR	Green/red	IR/red	IR/green
20°	10·2	6·0	34·5	1·7	5·8	3·4
75°	5·4	1·5	25·0	3·6	16·7	4·6

7.8 *Remote sensing of soils* (Montgomery *et al* 1976)

Many researchers have claimed that a close qualitative relationship exists between spectral response of soils and the composition of soils. Five soil parameters are highly correlated with spectral reflectance. These are cation exchange capacity (CEC), silt content, organic matter content, iron content (Fe_2O_3) and clay content. These studies have revealed further that (i) the chromaticity of the soils is directly related to the content of free iron and clay and inversely proportional to iron content. They have given the empirical relationship

$$\text{reflection at } 0{\cdot}64\ \mu\text{m in } \% = 85 - 4{\cdot}9\ (\text{content of } Fe_2O_3 \text{ in } \%).$$

This equation can be used to estimate iron in soils. Page (1974) has shown that the reflectance determined using a colour-difference meter is highly correlated with soil organic matter in coastal plain soils.

7.9 *Effect of particle size on reflectance*

Orlov (1966) has shown that the reflection coefficient R and aggregate diameter d of soil are related as

$$R = K \cdot 10^{-nd} + R_\infty,$$

where K, n, and R_∞ are constants. R_∞ is the reflection coefficient of aggregates of maximum diameter. It is also reported that the shape rather than the size of the particles

influences the reflection properties. This is because although part of the light flux incident upon an ideal surface of spherical particle is completely extinguished, the total reflectance is independent of the diameter of the spheres. As light falls on large, irregularly-shaped aggregates most of the eight flux penetrates into eight traps and is completely extinguished there. As a result reflectance decreases (see figure 13).

Montgomery *et al* (1976) has reported the following findings. (i) Silt content is the single most significant parameter in explaining spectral variations; (ii) organic matter content contributes significantly to the explanation of the variation in the visible spectral region; (iii) the iron content of the soil is significant in both visible and infrared regions. The significance of iron increases with increasing wavelengths; (iv) clay content is significant in the 0·5–0·7 μm region (v) CEC is highly correlated with spectral reflectance; (vi) biochemical properties are also highly correlated.

The above results indicate that there exists the potential for developing quantitative relationships between soil properties and reflectance. Such relationships will be immensely useful in predicting soil properties from the reflectances obtained by remote sensing.

8. Conclusion

The most successful series of remote sensing satellites has been the LANDSAT satellites. These have concentrated on land-based uses. The ocean has not received as much attention as is necessary. Other applications like cartography, have also not received much attention. This situation is sought to be remedied by the future programmes of the United States, Japan, Europe etc. A parallel move is the increase of resolution. The recently launched LANDSAT-4 carries a 7-band multispectral scanner with nearly double the resolution of LANDSAT-3 MSS. The French SPOT satellite will give stereoscopic images. It also has a higher resolution of 20 m. The United States will launch a STEREOSAT satellite which would acquire worldwide stereoscopic coverage through a single instrument system consisting of three cameras (Duchossois *et al* 1981).

The United States National Oceanic Satellite System (NOSS) satellite will carry a scatterometer, radar actimeter, scanning multichannel microwave radiometer, SMMR, coastal zone colour scanner, CZCS and advanced very high resolution radiometer, AVHRR. The Japanese MOS-1 (marine observation satellite system) will carry a multispectral electronic self-scanning radiometer (MESSR) visible and thermal-infrared radiometer (VTIR) and a microwave scanning radiometer (MSR). These instruments will give information regarding sea-surface colour, sea-surface temperature and water

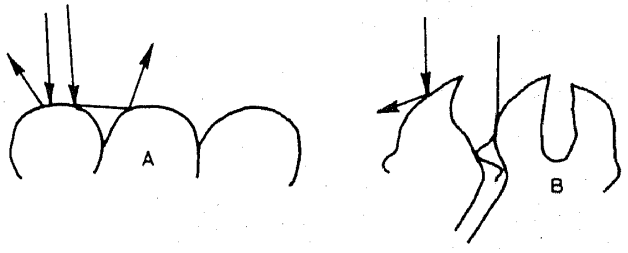

Figure 13. Diffuse reflection from the surface of aggregates (A) = spherical aggregates (B) = irregularly shaped aggregates

vapour content of atmosphere. The shuttle imaging radar (SIR), to be flown by NASA will carry an L-band synthetic aperture radar (SAR).

The United States will launch an ICE processes satellite (ICESAT) and an automated mapping satellite (MAPSAT).

A magnetic anomaly detection satellite (MAGSAT) was launched a few years ago. Other proposed satellites include those for measuring earth's gravity, geodynamic ranging, heat capacity, soil moisture etc.

In this paper we have listed some of the problems which affect the applicability of remotely-sensed data. The multiplicity of satellites listed above poses yet another problem; that of compatibility. At a minimum the satellite/ground station interfaces need to be to a common standard (*e.g.*, telemetry frequency bands, modulation techniques) and the HDDT (high density digital tape) recorders at the stations need to be capable of recording data from different satellites. The orbits of the satellites should be chosen so that coverage frequency is increased. Conversely the payloads can be made complementary to extend the range of applications (Duchossois *et al* 1981).

References

Baudolin A 1981 in *Remote sensing in meteorology, oceanography and hydrology* (ed.) A P Cracknell (England: Ellis Horwood)

Billingsley F C 1982 *J. Photogramm. Eng. Remote Sensing* **48** 421

Duchossois G & Plevin J 1981 in *Remote sensing in meteorology, oceanography and hydrology* (ed.) A P Cracknell (England: Ellis Horwood)

Fraser R S, Curran R J, Lintz J Jr & Simonett D S 1976 in *Remote sensing of environment* (Massachusetts, USA: Addison-Wesley)

Friedman H D 1966 *Proc. IEEE* **53** 658

Fu K S 1983 *Proc. Indian Acad. Sci. (Engg. Sci.)* **6** 153

Golwell J E 1974 Grass canopy bidirectional spectral reflectance, Environmental Research Institute of Michigan, Symposium, Ann Arbor, Michigan, USA

Hugli H & Frei W 1981 Correcting for anisotropic reflectances in remotely sensed images from mountainous terrains, Laboratory for the Application of Remote Sensing, Purdue University, Indiana, USA, Symposium

Krishnan R & Natarajan S 1978 Estimating proportions of classes in a boundary pixels, Environmental Research Institute of Michigan, Symposium, Manila

La Rocca A J 1975 *Proc. IEEE* **63** 1

Malila W A 1974 Analysis of multispectral signatures and investigation of multiaspect remote sensing techniques, NASA CRERIM 190 100–27-T

Montgomery O L, Baumgardner M F & Weismuller R A 1976 An investigation of the relationship between spectral reflectance and the chemical physical and genetic characteristics of soils, Laboratory for the Application of Remote Sensing, Note 082776

Nalepka R F, Horwitz H M & Hyde P D 1972 Estimating properties of objects from multispectral data, Report NASA CR WRL 31650–73 T. Willow Run L Laboratories, University of Michigan, Michigan, Ann Arbor, USA, 3/72

Orlav D S 1966 *Sov. Sci.* **13** 1495

Otterman J 1975 in *Remote sensing: Energy related studies* (ed.) T N Veziroglu (New York: John Wiley)

Page N R 1974 *Agron. J.* **66** 652

Randall C M 1975 *Opt. Engg. J. Infrared Atmospheric Effects*, **2** 55

Short N M 1975 in *Remote sensing energy related studies* (ed.) T N Veziroglu (New York: John Wiley)

Sturm B 1981 in *Remote sensing in meteorology, oceanography and hydrology* (ed.) A P Cracknell (England: Ellis Horwood)

Tepper M 1975 in *Remote sensing: Energy related studies* (ed.) T N Veziroglu (New York: John Wiley)

Tucker C J, Elgin Jr J H, McMurtrey III J E & Fan C J 1979 *Remote sensing Environ.* **8** 237